Real-time imaging of cell-cell adherens junctions reveals that *Drosophila* mesoderm invagination begins with two phases of apical constriction of cells

Hiroki Oda[1],* and Shoichiro Tsukita[1,2]

[1]Tsukita Cell Axis Project, Exploratory Research for Advanced Technology, Japan Science and Technology Corporation, Kyoto Research Park, Chudoji Minami-machi, Shimogyo-ku, Kyoto 600-8813, Japan
[2]Department of Cell Biology, Faculty of Medicine, Kyoto University, Yoshidakonoe-cho, Sakyo-ku, Kyoto 606-8501, Japan
*Author for correspondence (e-mail: hoda@cell.tsukita.jst.go.jp)

SUMMARY

Invagination of the epithelial cell sheet of the prospective mesoderm in *Drosophila* gastrulation is a well-studied, relatively simple morphogenetic event that results from dynamic cell shape changes and cell movements. However, these cell behaviors have not been followed at a sufficiently short time resolution. We examined mesoderm invagination in living wild-type embryos by real-time imaging of fluorescently labeled cell-cell adherens junctions, which are located at the apical zones of cell-cell contact. Low-light fluorescence video microscopy directly visualized the onset and progression of invagination. In an initial period of approximately 2 minutes, cells around the ventral midline reduced their apical surface areas slowly in a rather synchronous manner. Next, the central and more lateral cells stochastically accelerated or initiated their apical constriction, giving rise to random arrangements of cells with small and relatively large apices. Thus, we found that

mesoderm invagination began with slow synchronous and subsequent fast stochastic phases of cell apex constriction. Furthermore, we showed that the mesoderm invagination of *folded gastrulation* mutant embryos lacked the normal two constriction phases, and instead began with asynchronous, feeble cell shape changes. Our observations suggested that Folded gastrulation-mediated signaling enabled synchronous activation of the contractile cortex, causing competition among the individual mesodermal cells for apical constriction.

Movies available on-line:
http://www.biologists.com/JCS/movies/jcs2073.html

Key words: Mesoderm, Invagination, Gastrulation, Apical constriction, Adherens junction, Cadherin, Folded gastrulation, GFP, *Drosophila melanogaster*

INTRODUCTION

Invagination or folding of an epithelial cell sheet is seen in a variety of morphogenetic events in metazoan development. Such epithelial morphogenesis often begins with constriction of the apices of specific cell populations. For example, avian neural tube formation and amphibian bottle cell formation, which have been analyzed extensively, initially exhibit cells with small apices in defined regions of the epithelia (Schoenwolf and Franks, 1984; Hardin and Keller, 1988). Constriction of cell apices appears to play an important role in the initiation of epithelial invagination or folding.

Invagination of the prospective mesoderm in *Drosophila* gastrulation is a well-studied morphogenetic event that begins with constriction of cell apices. At about 3 hours of development, a *Drosophila* embryo has about 6000 cells, all of which, with the exception of the germ cells, are essentially uniform in size and shape, and are organized in an epithelial layer. In the cellular blastoderm, a band of cells corresponding to the ventral one-quarter of the embryo (approximately 18 cells in width) is destined to be the mesoderm. The prospective mesoderm begins morphogenetic movement earlier than all other regions of the embryo, and is brought into the interior of

the embryo within 20 minutes at 25°C. Although there have been many detailed studies of the morphology of the mesodermal cells during the invagination (Turner and Mahowald, 1977; Fullilove et al., 1978; Leptin and Grunewald, 1990; Kam et al., 1991; Parks and Wieschaus, 1991; Sweeton et al., 1991; Costa et al., 1993; Oda et al., 1998), most were performed with fixed embryos. Detailed observations using scanning electron microscopy and epi-illumination video microscopy (Sweeton et al., 1991) suggested that the process of mesoderm invagination is divided into four phases: (1) flattening of the cell apices and initial random apical constrictions; (2) a shallow groove stage associated with increased constriction and cell elongation; (3) cell shortening and the subsequent inward movement; (4) closing over of the invagination and germband extension. In addition, examination of living embryos using a combination of injection of fluorescent reagents that visualize cell outlines and nuclei, and time-lapse three-dimensional fluorescence microscopy, supported the idea of initial random initiation of cell shape changes and the subsequent groove formation stage, although the data sets were only acquired at 1-minute intervals (Kam et al., 1991). It was also suggested that cell-cell communication mediated by Folded gastrulation may involve a rapid, orderly

progression of constriction initiations from the center to the periphery of the mesoderm (Costa et al., 1994). These earlier observations implied that the mesodermal cell behavior during gastrulation is too dynamic to be thoroughly described without examining living embryos at much higher time resolutions.

The classic cadherin-based cell-cell adhesion system has been shown to play a fundamental role in controlling cell behavior during morphogenesis of both vertebrates and invertebrates (Tepass, 1999; Steinberg and McNutt, 1999). In epithelial cells of embryos or tissues, E-type classic cadherin, a membrane-spanning protein, constitutes cell-cell adherens junctions together with many other components including β- and α-catenin (Yap et al., 1997; Steinberg and McNutt, 1999; Provost and Rimm, 1999). The adherens junctions, linking apical edges of epithelial cells, interact with cortical actin bundles (Provost and Rimm, 1999), and are thought to contribute mechanically to the constriction of cell apices in epithelial invagination or folding. In the *Drosophila* cellular blastoderm, adherens junctions are formed in the apical areas of the lateral surfaces of the cells (Tepass and Hartenstein, 1994). *Drosophila* E-cadherin (*D*E-cadherin) is present in the adherens junctions together with Armadillo and *D*α-catenin (Oda et al., 1993; Oda et al., 1994; Müller and Wieschaus, 1996). In the ventralmost prospective mesodermal cells that have just begun to constrict their apices, adherens junctions are observed at the apical poles of the lateral cell surfaces (Oda et al., 1998). As the invagination proceeds, the adherens junctions appear to be disrupted in parallel with transition of the mesodermal cells from the epithelial to the mesenchymal state. Contraction of a cortical actin-myosin network may mediate apical constriction at the start of mesoderm invagination (Young et al., 1991; Leptin et al., 1992). Concertina (G protein α-subunit), DRhoGEF2 (guanine nucleotide exchange factor) and Rho1 (GTPase) may be involved in the Folded gastrulation (Fog) signaling pathway, which coordinates cell shape changes (Parks and Wieschaus, 1991; Costa et al., 1994; Barrett et al., 1997; Häcker and Perrimon, 1998).

In this study, we expressed *D*E-cadherin tagged with green fluorescent protein in early *Drosophila* embryos to enable real-time imaging of cell-cell adherens junctions before and during gastrulation. Low-light fluorescence video microscopy, with which we recorded images every second, directly visualized the onset of mesoderm invagination in addition to the rest of this event in wild-type embryos. Our observations revealed dynamic aspects of cell behavior, some of which might be difficult to recognize clearly in low-time resolution analyses. We found that *Drosophila* mesoderm invagination began with slow synchronous and subsequent fast stochastic phases of cell apex constriction. Furthermore, we observed defective cell behavior of the prospective mesoderm in living *fog* mutant embryos, directly demonstrating the importance of Fog-mediated signaling in the two phases of cell apex constriction.

MATERIALS AND METHODS

DNA constructs and transgenic flies

cDNA containing the open reading frame and the 3′ untranslated region for *D*E-cadherin was modified by addition of a *Bsp*HI site at the translational start site and of a *Nco*I site in front of the stop codon, and cloned into the *Nco*I/*Xba*I site of pUP2M, which contains the promoter region of the *ubiquitin* gene (Lee et al., 1988). The resulting plasmid was named pUP-DECH-Nc. A red-shifted mutant GFP cDNA (pQBI25, excitation peak 473 nm; emission peak 509 nm, Quantum Biotechnologies) was inserted into the *Nco*I site of pUP-DECH-Nc, and then the *Kpn*I-*Xba*I fragment was transferred to pCaSpeR4-SV40 (Oda and Tsukita, 1999) to produce pCaSpeR-ubi-DE-cad-GFP. Transgenic flies were produced as described previously (Robertson et al., 1988). Several independent homozygous lines were established, and examined with a Zeiss Axiophot II microscope or an Edge direct-view 3-D microscope. In all the lines, cell-cell adherens junctions were clearly visible. Although the selected line of *ubi-DE-cad-GFP* laid many unfertilized eggs (about 50%) for as yet unknown reasons, most fertilized eggs from the flies developed normally.

Western blotting and antibodies

For western blotting, anti-*D*E-cadherin (Oda et al., 1994), anti-α-spectrin (Pesacreta et al., 1989) and anti-GFP (Clontech) antibodies were used at dilutions of 1:50, 1:1000 and 1:1000, respectively.

Flies

Canton-S was used as the wild-type *Drosophila melanogaster* strain. $Df(2R)E2$, shg^{R69} and fog^{4a6} were described previously (Uemura et al., 1996; Godt and Tepass, 1998; Costa et al., 1994). The recombinant, $Df(2R)E2$, *ubi-DE-cad-GFP*, did not complement $Df(2R)E2$, $Df(2R)D17$, $insc^{P49}$ or $insc^{P72}$ (Uemura et al., 1996; Kraut and Campos-Ortega, 1996), but did complement shg^2, shg^{g317} and shg^{E17B} in addition to shg^{R69} (Uemura et al., 1996; Tepass et al., 1996).

Southern blotting

Genomic DNA was isolated from adult flies with the indicated genotypes, and digested with *Hin*dIII. Digoxigenin (DIG)-labeled nucleotide probes were generated using a PCR DIG Probe Synthesis Kit (Boehringer Mannheim), and used for hybridization. Signals were detected using a combination of peroxidase-conjugated anti-DIG antibody (Boehringer Mannheim) and the ECL detection system (Amersham Pharmacia Biotech).

Video microscopy

ubi-DE-cad-GFP embryos at 2.5 hours of development (25°C) were dechorionated, placed on coverslips in the appropriate orientation, set in place with vacuum silicone grease (Beckman) and mounted in halocarbon oil 700 (Sigma) on special slides with an oxygen-permeable membrane (Yellow Spring Instrument) as described (Girdham and O'Farrell, 1994). The embryos were then viewed under an inverted fluorescence microscope (Carl Zeiss, Axiovert 135) equipped with a highly sensitive SIT video camera (C2741-08, Hamamatsu Photonics) using a 100× NA1.4 Plan-Apochromat oil immersion objective (Carl Zeiss) and a filter set for GFP (Chroma, 41017). Excitation light generated from a 100 W mercury arc fluorescent-light source was attenuated to 1.5-6% using 50, 25 and 12% ND filters. Images were subjected to real-time averaging by Argus 20 (FRM=32, Hamamatsu Photonics), and recorded every second on a laser disc using a laser videodisc recorder (LVR-3000AN, Sony). During the 30-60 minute period of observation of embryos at 23±1°C, the focus was manually adjusted to the level of the embryo surface. The observed embryos were further incubated to check that they developed normally to hatching. Some images were transferred to a Power Macintosh, and processed using Adobe Potoshop 4.0J, NIH image 1.61 and Adobe Premiere 4.2.1J to produce the figures and the QuickTime movies. Measurement of area was performed using Adobe Photoshop 4.0J.

To observe *fog* mutant embryos, a confocal microscope (Bio-rad, MRC1024) was used. Images were taken at 10 second intervals with 3% of the maximum laser power. This condition did not affect gastrulation and germband extension in wild-type embryos. Embryos from *fog^{4a6}/FM7 and Y/FM7; ubi-DE-cad-GFP* were randomly taken and observed. During and after the observations, we ascertained

whether the individual embryos exhibited characteristic *fog* phenotypes as described previously (Costa et al., 1994).

RESULTS AND DISCUSSION

Visualization of adherens junctions in living early embryos

To visualize the adherens junctions in living *Drosophila* embryos, we constructed a chimeric gene encoding *D*E-cadherin tagged at its C terminus with green fluorescent protein (*D*E-cadherin-GFP), and used it to transform flies. The constructed gene, designated as *ubi-DE-cad-GFP*, contained the *ubiquitin* promoter (Lee et al., 1988) (Fig. 1A), which allowed ubiquitous expression of the gene product throughout development. We established several independent homozygous lines, each of which had two copies of *ubi-DE-cad-GFP* in addition to two copies of the endogenous *D*E-cadherin gene, encoded in the *shotgun (shg)* locus (Uemura et al., 1996; Tepass et al., 1996), and designated these flies as *ubi-DE-cad-GFP*. Of these, we selected one line not only bearing the transgene on the second chromosome, where *shg* is located, but also expressing *D*E-cadherin-GFP at a level comparable to that of endogenous *D*E-cadherin (Fig. 1B), and used it throughout this study. When living *ubi-DE-cad-GFP* embryos were examined by fluorescence microscopy, cell-cell adherens junctions, which form three-dimensional networks linking apical edges of epithelial cells, were clearly visible in blastoderm cells and later epithelial cells (Fig. 2).

ubi-DE-cad-GFP complements the *shg* null mutant

We next examined whether *ubi-DE-cad-GFP* can function in development. Zygotic mutations in *shg* lead to severe defects in morphogenetically active epithelia of the embryo (Uemura et al., 1996; Tepass et al., 1996). To perform rescue assays of *shg* mutants with *ubi-DE-cad-GFP*, we generated a chromosome containing *ubi-DE-cad-GFP* and a deletion, *Df(2R)E2*, which removes at least *shg* and a nearby essential gene, *inscuteable (insc)* (Uemura et al., 1996; Kraut and Campos-Ortega, 1996). Flies with this chromosome were crossed with those carrying a *shg* null allele, *shg^{R69}* (Godt and Tepass, 1998), to produce embryos with the zygotic genotype of *Df(2R)E2, ubi-DE-cad-GFP/shg^{R69}*. These embryos developed into morphologically normal adult flies, the genotype of which was confirmed by Southern blotting (Fig. 1C). In addition, the progeny of *Df(2R)E2, ubi-DE-cad-GFP/shg^{R69}* flies were maintained for more than 5 generations, and homozygotes for *shg^{R69}*, *ubi-DE-cad-GFP* developed normally. These results indicated that *ubi-DE-cad-GFP* complemented the *shg* null allele, and that *D*E-cadherin-GFP

Fig. 1. Construction and characterization of *ubi-DE-cad-GFP*. (A) Schematic representation of the structures of the *shg* and *ubi-DE-cad-GFP* genes and the *D*E-cadherin-GFP protein. Arrowheads indicate cleavage sites for maturation of *D*E-cadherin (Oda and Tsukita, 1999). Matured *D*E-cadherin-GFP consists of a 150 kDa polypeptide containing the CRs and a 110 kDa polypeptide containing the GFP, noncovalently bound to each other. CRs, cadherin repeats; NC, nonchordate motif; CE, cysteine-rich EGF-like motif; LAG, laminin A globular domain-like motif; PCCD, primitive classic cadherin domain; CP, cytoplasmic domain. (B) Western blot analysis of *D*E-cadherin-GFP. Lysates of 4-6 hour embryos of the wild-type (Wt) and *ubi-DE-cad-GFP* were resolved on 7.5% SDS gels. The indicated number of embryos was loaded in each lane. The antibodies used are indicated to the right of each blot. Anti-α-spectrin antibody (Anti-αSp) was used as a control to check that the expected amounts of protein were loaded in each lane. The squares indicate the precursor form of endogenous *D*E-cadherin, whereas the asterisks indicate the precursor form of *D*E-cadherin-GFP. As judged by the intensities of the detected bands, the quantity of the product from the *ubi-DE-cad-GFP* gene was comparable to that from the *shg* gene. (C) Southern blotting analysis of *Hind*III-digested genomic DNA derived from wild-type (lane 1), *Df(2R)E2/CyO* (lane 2), *Df(2R)E2, ubi-DE-cad-GFP/CyO* (lane 3) and *Df(2R)E2, ubi-DE-cad-GFP/shg^{R69}* (lane 4) adult flies. The probe and *Hind*III sites are shown in A. The lower bands (2.5 kb) correspond to *shg*, and the upper bands (4.5kb) to *ubi-DE-cad-GFP*.
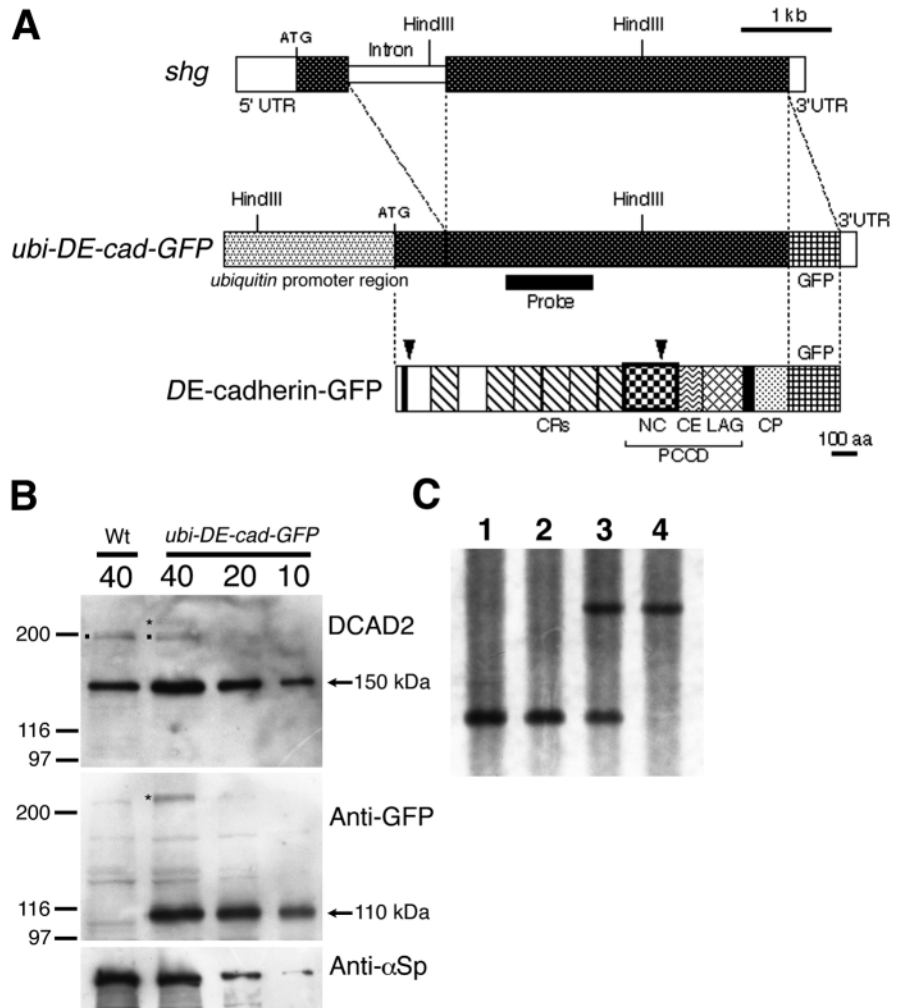
Fig. 2. Visualization of cell-cell adherens junctions in a living early embryo. A stereo micrograph of a lateral view of a stage 8 *ubi-DE-cad-GFP* embryo revealing a three-dimensional network of cell-cell adherens junctions linking apical edges of surface epithelial cells. As, apical surface; gb, germband. Bars, 20 μm.
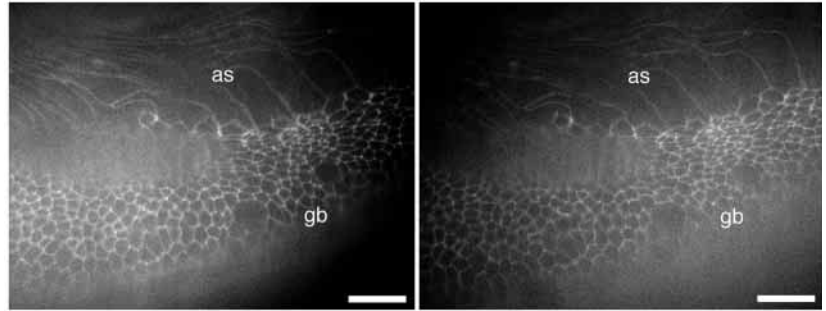
can function normally even in the complete absence of intact *D*E-cadherin. Also, it was suggested that the behavior of *D*E-cadherin-GFP, visible as fluorescence in the living flies, is the same as that of intact *D*E-cadherin. *ubi-DE-cad-GFP*, therefore, could be an ideal tool not only for visualizing the adherens junctions but also for analyzing the dynamics of the functional cadherin molecule.

Video microscopy revealed the time course of changes in cell shape and cell movements during mesoderm invagination

To follow the changes in shape and position of the prospective mesodermal cells before and during gastrulation, we examined living *ubi-DE-cad-GFP* embryos. A highly sensitive video camera enabled us to detect sufficient levels of GFP signals continuously with excitation light largely attenuated by ND filters. Exposure of early embryos to the excitation light for 30-60 minutes did not affect gastrulation or later development. Blastoderm embryos were mounted on slides so that their ventral side, corresponding to the prospective mesoderm region, faced the objective lens (Fig. 3A). Since the mounted embryos were slightly flattened by compression, a larger part of the embryo surface was set in focus than in intact embryos. This deformation did not essentially affect cell behaviors in the developing embryos. The observed embryos on the slides developed normally to hatching, suggesting that they had undergone no serious damage while being observed. Images were recorded every second from before the onset of gastrulation to the start of germband extension, at 23±1°C. We obtained four sets of sequential images from different embryos, and found that they showed consistent results with only small variations. Of the four, a representative set of images is shown in Fig. 3B. We traced back the cells positioned at the site of ventral closure, corresponding to the mesectodermal cells, and determined which cells were destined to form the mesoderm. The prospective mesodermal cells, positioned more ventrally than the mesectodermal cells, showed dynamic changes in shape and position. Onset of movement in the prospective mesoderm was detected around a time point corresponding to the third panel of Fig. 3B in a quantitative analysis described below (Fig. 4), and this time point was therefore designated time 0.

The process of mesoderm invagination was roughly divided into the following four stages. First, the majority of cells in the centralmost (or midventral) region, corresponding to about two thirds of the total mesoderm, constricted their apices, while the apices of more lateral mesodermal cells, designated as the lateral mesodermal cells, were elongated along the mediolateral axis (Fig. 3B, 0-7 minutes). *D*E-cadherin-GFP

was strongly concentrated at the reduced apical zones of cell-cell contact. This constriction stage was subdivided into slow and fast phases on the basis of the analysis described below. Second, the midventral cells gradually moved apart from the tangential plane to form a shallow furrow, called the ventral furrow, along the anterior-posterior axis (Fig. 3B, 7-14 minutes). Many of the lateral mesodermal cells were still in the exterior, while their apices were further elongated. Third, the lateral mesodermal cells rapidly migrated toward the ventral midline, and then entered the interior of the embryo, presumably pushing the midventral cells inward (Fig. 3B, 14-20 minutes). Finally, the prospective mesectodermal cells coming from both sides met at the ventral midline, and maximized their contacts, where *D*E-cadherin-GFP was accumulated (Fig. 3B, 20-25 minutes). This sealing of the ventral midline by the mesectodermal cells was accompanied by the start of germband extension.

Most published images of fixed embryos at various gastrulation stages could be correlated with the images obtained here. Our observations, therefore, provide an example of time scales for cell shape changes and cell movements during mesoderm invagination, although the timing of the cellular behaviors varied slightly between embryos. The stages defined above may be comparable to those defined previously using a combination of epi-illumination video microscopy and scanning electron microscopy (Sweeton et al., 1991).

Quantitative analysis revealed slow and fast phases of cell apex constriction following the onset of mesoderm invagination

The prospective mesodermal cells in the cellular blastoderm were essentially uniform in shape and area, with only small variations. We found no cells that increased or decreased their apical surface areas at a significant rate in an irreversible manner before the onset of mesoderm invagination. After only 5 minutes, however, the apical surfaces of the mesodermal cells exhibited large differences in shape and area, as they began to change their shapes (Fig. 3B). To examine the relationship between the position of the mesodermal cells relative to the medio-lateral axis and the timing of their shape changes, we identified four adjoining groups each containing ten cells in mediolateral order as shown in Fig. 4A, and followed the temporal changes in the apical surface area of each group (Fig. 4B). The most ventral group, Group 1, began to show a reduction of the apical area earlier than all the other groups. The adjacent, more lateral group, Group 2, showed a rapid reduction in apical area with a delay of about 2.5 minutes. In contrast to Groups 1 and 2, Group 3 showed a significant increase in apical area followed by a rapid reduction in the area.
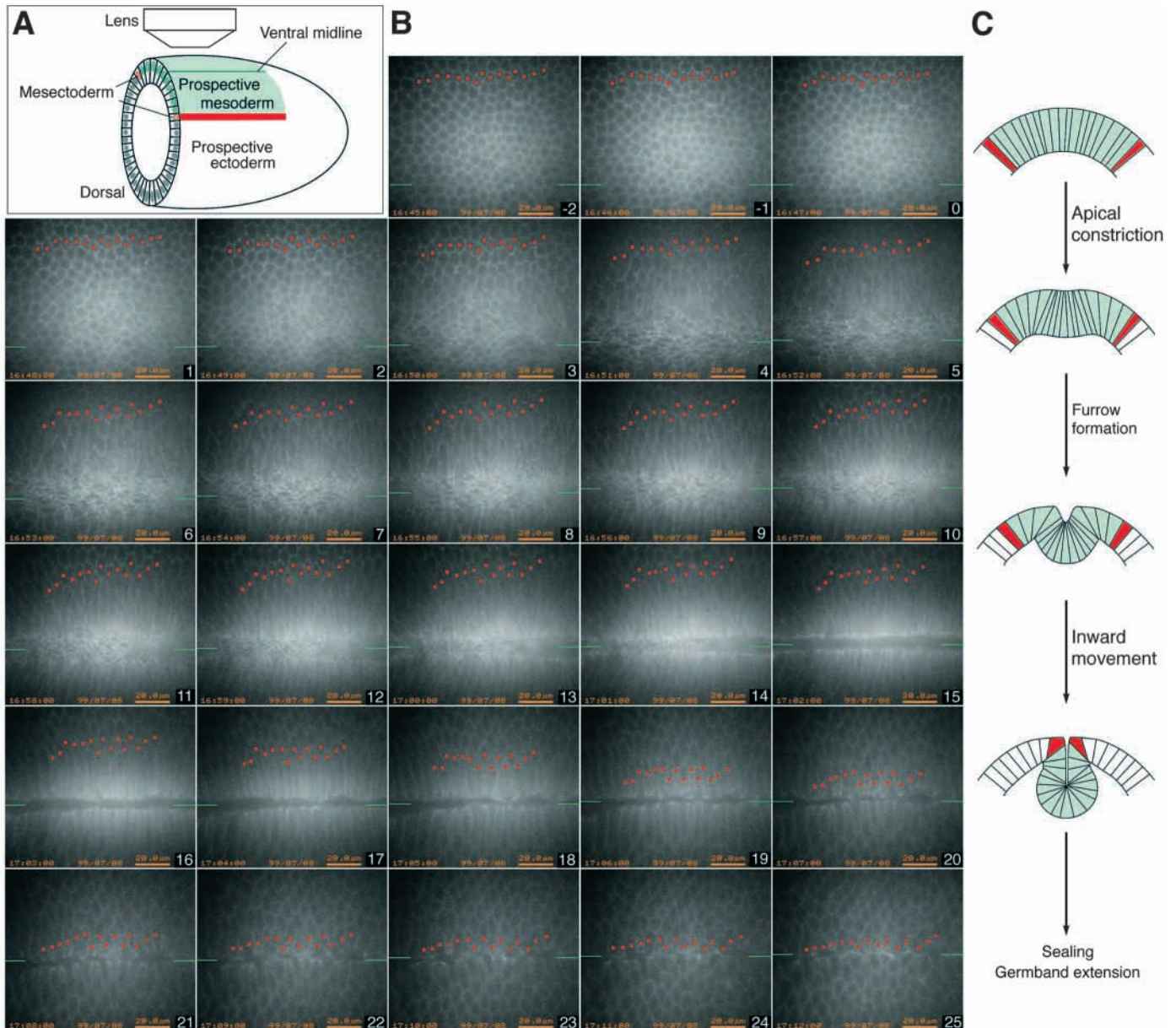
Fig. 3. Video microscopic observation of mesoderm invagination. The surface of a living *ubi-DE-cad-GFP* embryo was observed by low-light video microscopy. Images were recorded at 1 second intervals. (A) Schematic illustration showing the prospective mesodermal region of the embryo. Red dots indicate mesectodermal cells and green lines the ventral midline. (B) Images were selected at 1-minute intervals. Time (minutes) is indicated at the bottom of each panel. Time 0 corresponds to the onset of mesoderm invagination detected quantitatively (see Fig. 4B). The ventral midline is marked by green bars. 15 mesectodermal cells were traced back, and are marked by red dots. The anterior is to the left. See also Movie 1. (C) Schematic illustration of cross-sections of gastrulating embryos corresponding to the images shown in B.

The most lateral group, Group 4, did not decrease but increased its apical area from the onset of apical constriction, eventually reaching a plateau. These observations indicated that apical constrictions start first in the center of the mesoderm followed by lateral propagation of apical constrictions, while the most lateral cells (about 3 cells in width) are forced to enlarge their apical surfaces.

The behavior of the cells around the ventral midline, including those in Group 1, involved two phases of apical constriction. During the first phase, lasting for about 2 minutes, the apical area of Group 1 decreased slowly with only slight differences between the individual cells (Fig. 4A,B). Most cells

in the central region reduced their apical areas. No cells were found that showed rapid constriction of their apices compared to their surrounding cells. During the second phase, the apical area of Group 1 decreased about 2.5-fold faster than in the preceding phase, and the differences between the cells became progressively apparent (Fig. 4B,C). Many, but not all, cells around the ventral midline showed accelerated constriction of their apices. Many rapidly constricting cells were also found in Group 2 and in similar positions, with fewer in positions corresponding to Group 3 during the second phase (Fig. 4A). In contrast to the rapidly constricting cells, the remaining cells failed to accelerate their constriction, and some were slightly
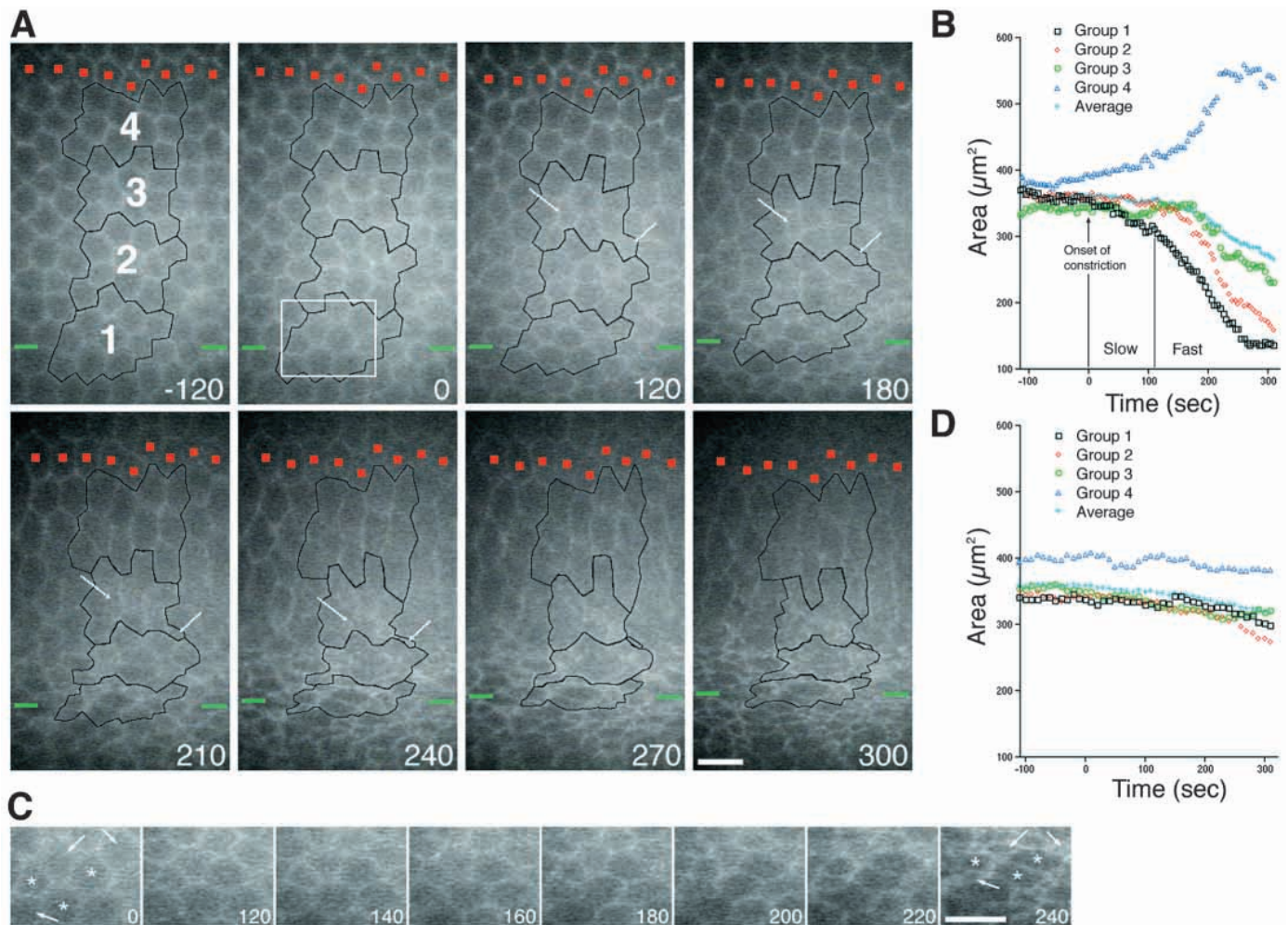
Fig. 4. Cell behavior at the start of mesoderm invagination. (A) High magnification images from the same set of data as used for Fig. 3. Four adjoining groups each consisting of 10 cells were set in the prospective mesodermal region, and numbered 1 to 4 in order of mediolateral position, as shown in the first panel. The outline of each group was drawn on the images selected at 5-second intervals, and some of the drawings are shown here. Time (seconds) is indicated at the bottom of each panel. Color code is the same as in Fig. 3B. Arrows indicate two examples of cells constricting their apices rapidly in Group 3. (B) Temporal changes in the apical surface area of each group. (C) Random arrangement of cells with small (arrows) and relatively large (asterisks) apices became progressively apparent during the fast phase. The images shown correspond to the boxed region in A, panel 0. See also Movie 2. (D) Temporal changes in the apical surface area of each group in a *fog* mutant embryo shown in Fig. 5A. Bars, 10 μm.

widened, coinciding with constriction of nearby cells (Fig. 4C), although they soon began again to reduce their apical areas. In the middle of the second phase, cells with small and others with relatively large apices were randomly arranged, and the individual embryos showed different patterns. In all the embryos observed, cell behaviors characteristic of both the slow and fast phases were observed. These observations suggested that the onset of mesoderm invagination was followed by slow synchronous and subsequent fast stochastic phases of cell apex constriction.

Fig. 5. Defective cell behavior in a *fog* mutant embryo at the start of mesoderm invagination. (A) The surface of an embryo with the genotype of *fog/Y*; *ubi-DE-cad-GFP* was observed by time-lapse confocal microscopy. Images were recorded at 10-second intervals, and are shown here at 1-minute intervals. Time (minutes) is indicated at the bottom of each panel. Color code is the same as in Fig. 3B. Anterior is to the left. The cell groups (the apical surface areas of which were measured for Fig. 4D) are indicated in the first panel. The brackets indicate a central 8 cell-wide region corresponding to Groups 1 and 2. Five cells are arbitrarily marked by + to make it easier to follow changes in cell arrangement. From around time 0, reductions in the surface areas of the central cell groups were quantitatively detected (Fig. 4D). In the central 8-cell-wide region, some cells in random positions began to constrict their apices very slowly (arrows), and other cells remained large with no initial constriction (asterisks). Some of the constricted cells enlarged their apices again later (arrows). In this example, onset of folding took place from an anterior region of the embryo (large arrow in the panel 12), while many of the central cells still had large apices. As a result, in panel 13, the apices of the cells marked by the asterisks were forced to become enlarged or distorted. Note that the shapes of lateral mesodermal cells were less affected by the constriction of central cells at earlier time points compared to normal embryos. (B) Normal embryo with the genotype of either *fog/FM7* or *FM7/Y*; *ubi-DE-cad-GFP*. Anterior is to the right. In this embryo, all the central mesodermal cells reduced their apices to a sufficiently small size before the cell sheet folded. See also Movies 3 and 4. Bars, 20 μm.
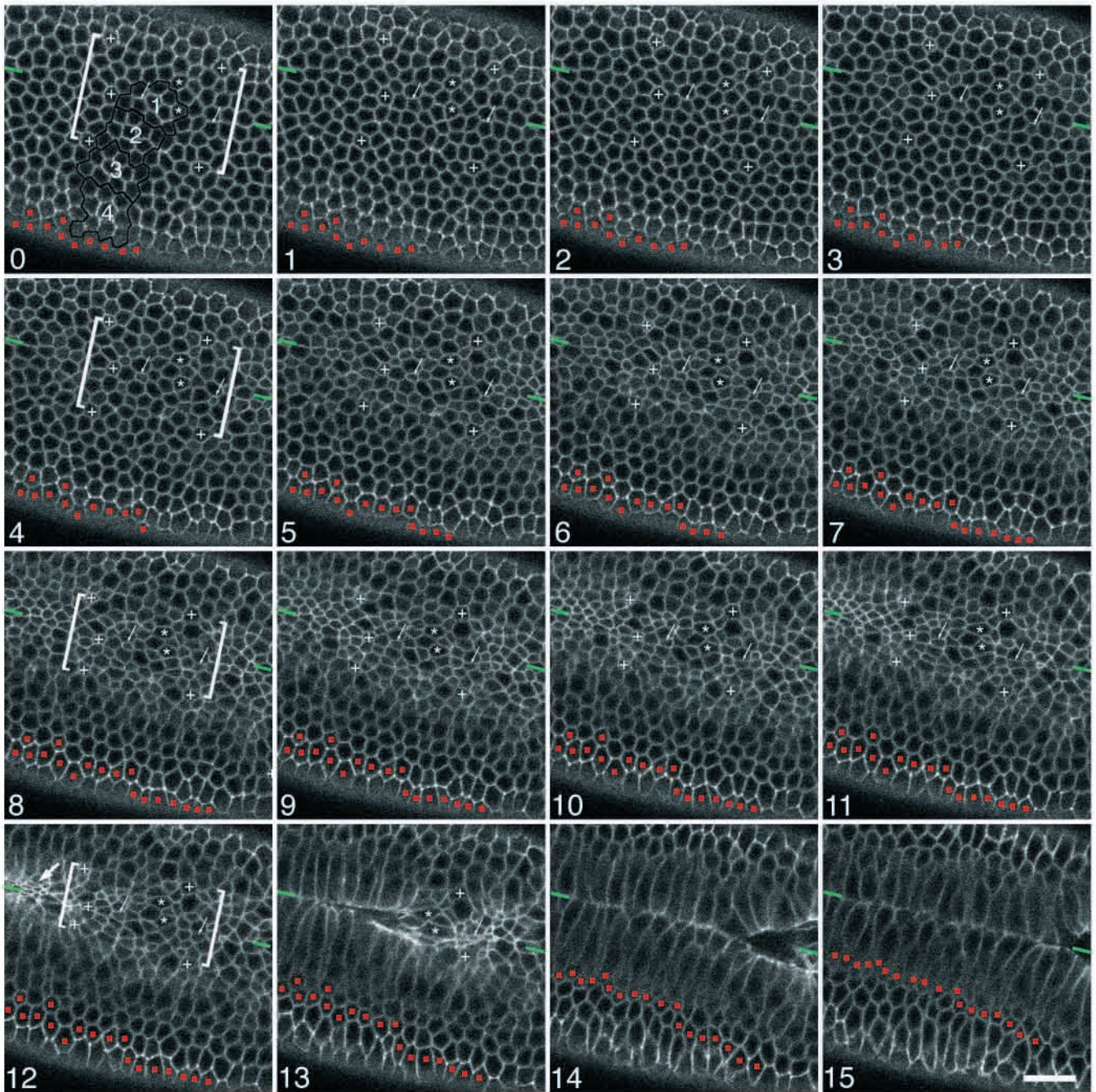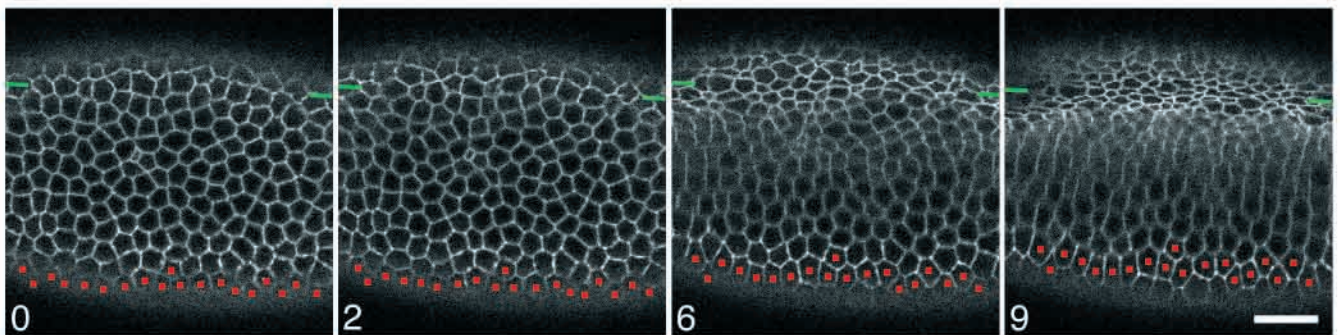
Some previous observations of living and fixed embryos suggested that mesoderm invagination begins with random initiation of apical constriction of individual cells (Sweeton et al., 1991; Kam et al., 1991). However, we found no cells showing prominently distinct behaviors from those of surrounding cells just after the onset of mesoderm invagination. In the initial 2 minutes, the cell shape changes were slight, and might be difficult to recognize in fixed embryo preparations or in low-time resolution analyses. Our observations suggested that the random apical constrictions observed previously (Sweeton et al., 1991) corresponded to the second phase of apical constriction defined in this study. It was previously shown that basal migration of the nuclei of the mesodermal cells also occurs in a random manner at the beginning of mesoderm invagination (Kam et al., 1991), but the relationship between apical constriction and nuclear migration was not analyzed in this study.

Defects of *fog* mutant embryos in the apical constriction

We introduced *ubi-DE-cad-GFP* into *fog* mutant embryos, in which ventral furrow formation was previously shown to be disordered (Costa et al., 1994), and observed the behavior of the prospective mesodermal cells in the living mutant embryos. We took images at 10 second intervals using time-lapse confocal microscopy, and present some of the images obtained from a *fog* mutant embryo together with those from a normal embryo in Fig. 5. In *fog* mutant embryos, the onset of mesoderm invagination was recognized when some cells randomly positioned in a central 8-cell-wide region corresponding to Groups 1 and 2 began to constrict their apices very slowly (Fig. 5A, arrows). The apices of many other cells in the central region remained large with no initial constriction (Fig. 5A, asterisks). The temporal changes in the apical areas of the cell groups were measured as was done for the normal embryo (Figs 4D, 5A). Even when the apical areas of the central mesodermal cells became varied, only slight decreases in the apical areas of Groups 1 and 2 were detected. Several minutes after the onset of mesoderm invagination, a random arrangement of cells with apices of various sizes became more apparent (Fig. 5A, 4-7 minutes). This mode of cell shape change was in contrast to that seen in wild-type embryos, in which stochastic acceleration of constriction of cell apices took place. Although the numbers of cells with relatively small apices slowly increased, the cell shape changes were reversible in *fog* mutant embryos. Some of the constricted cells enlarged their apices again later (Fig. 5, arrows). In addition, the apices of the lateral mesodermal cells were little enlarged in at least the first 6 minutes (Figs 4D, 5A), indicating that the total contraction force generated in the central mesodermal cells may be markedly weak. Although the initiation of folding of the mesodermal cell sheet was delayed in *fog* mutant embryos, when it did suddenly take place the apices of most central mesodermal cells were not fully constricted. During the folding, some cells around the ventral midline were forced to expand their apices (Fig. 5, asterisks). Thus, the prospective mesoderm of *fog* mutant embryos lacked the normal two constriction phases seen in wild-type embryos, and instead exhibited weak, asynchronous cell shape changes.

Fog is a secreted protein that may function as a signal to induce apical constriction of neighboring cells (Costa et al.,

1994; Morize et al., 1998). Our high-temporal resolution observations of wild-type and *fog* mutant embryos support the idea that Fog-mediated signaling enables synchronous initiation of the contraction forces exerted in central populations of the prospective mesodermal cells and rapid propagation of this initiation of contraction to more lateral cells. Without Fog activity, some prospective mesodermal cells did initiate apical constrictions, although their cell shape changes were feeble. The constrictions in *fog* mutants were likely to be caused by relatively weak contraction forces continuously or discontinuously generated in the cells in a rather independent manner. In *fog* mutant embryos, failure to minimize the apical areas of the central mesodermal cells resulted in an abnormal mode of folding of the mesodermal sheet.

Some previous studies stressed independent initiation of apical constriction in the individual cells (Sweeton et al., 1991; Kam et al., 1991). However, our observations suggest the importance of a Fog-mediated mechanism by which the central mesodermal cells synchronously initiate contraction forces to drive apical constriction at the onset of invagination. These contraction forces may give rise to high levels of tension among the central mesodermal cells. The apical area of each cell may depend on the balance between the force generated in the cell and that pulled from the surrounding cells. The irregular changes in cell shape observed in the second phase of apical constriction may result from imbalance of the elevated contraction forces among the individual cells rather than from random initiations of apical constriction. In other words, the synchronous activation of the contractile cortex by Fog-mediated signaling may cause competition among the individual mesodermal cells for apical constriction. During the second phase, lateral progression of initiation of apical constriction was detected by quantitative analysis (Fig. 4B). The changes in the apical areas of the grouped cells partially mimicked the situation proposed in the 'purse-string' model, in which a wave of contractions propagating from cell to cell is postulated (Odell et al., 1981).

This study enabled real-time imaging of cell-cell adherens junctions by making flies with ubiquitous expression of GFP-tagged *D*E-cadherin. We used these flies to examine dynamic cell behavior in *Drosophila* mesoderm invagination in wild-type and mutant embryos. The new tools are easily applicable to phenotypic analysis of other *Drosophila* mutants that have defects in epithelial cell polarity and morphogenesis. This kind of analysis may allow one to detect the earliest defects in such mutants, contributing to a better understanding of the molecular and cellular mechanisms controlled by the genes.

REFERENCES

Barrett, K., Leptin, M. and Settleman, J. (1997). The Rho GTPase and a putative RhoGEF mediate a signaling pathway for the cell shape changes in *Drosophila* gastrulation. *Cell* **91**, 905-915.

Costa, M., Sweeton, D. and Wieschaus, E. (1993). Gastrulation in

Drosophila: Cellular mechanisms of morphogenetic movements. *The Development of* Drosophila melanogaster (ed. M. Bate and A. Martinez-Arias), pp. 425-465. Cold Spring Harbor: Cold Spring Harbor Laboratory Press.

Costa, M., Wilson, E. T. and Wieschaus, E. (1994). A putative cell signal encoded by the *folded gastrulation* gene coordinates cell shape changes during *Drosophila* gastrulation. *Cell* **76**, 1075-1089.

Fullilove, S. L., Jacobson, A. G. and Turner, F. R. (1978). Embryonic development: descriptive. In *Genetics and Biology of Drosophila,* vol. 2c (ed. M. Ashburner and T. R. F. Wright), pp. 105-143. New York: Academic Press.

Girdham, C. H. and O'Farrell, P. H. (1994). The use of photoactivatable reagents for the study of cell lineage in *Drosophila* embryogenesis. In *Methods in Cell Biology* (ed. L. S. B. Goldstein and E. A. Fyrberg), pp. 533-543. San Diego: Academic Press.

Godt, D. and Tepass, U. (1998). *Drosophila* oocyte localization is mediated by differential cadherin-based adhesion. *Nature* **395**, 387-391.

Häcker, U. and Perrimon, N. (1998). DRhoGEF2 encodes a member of the *dbl* family of oncogenes and controls cell shape changes during gastrulation in *Drosophila*. *Genes Dev.* **12**, 274-284.

Hardin, J. and Keller, R. (1988). The behaviour and function of bottle cells during gastrulation of *Xenopus laevis*. *Development* **103**, 211-230.

Kam, Z., Minden, J. S., Agard, D. A., Sedat, J. W. and Leptin, M. (1991). *Drosophila* gastrulation: analysis of cell shape changes in living embryos by three-dimensional fluorescence microscopy. *Development* **112**, 365-370.

Kraut, R. and Campos-Ortega, J. A. (1996). *inscuteable*, a neural precursor gene of *Drosophila*, encodes a candidate for a cytoskeleton adaptor protein. *Dev. Biol.* **174**, 65-81.

Lee, H. S., Simon, J. A. and Lis, J. T. (1988). Structure and expression of ubiquitin genes of *Drosophila melanogaster*. *Mol. Cell Biol.* **8**, 4727-4735.

Leptin, M., Casal, J., Grunewald, B. and Reuter, R. (1992). Mechanisms of early *Drosophila* mesoderm formation. *Development* Supplement, 23-31.

Leptin, M. and Grunewald, B. (1990). Cell shape changes during gastrulation in *Drosophila*. *Development* **110**, 73-84.

Morize, P., Christiansen, A. E., Costa, M., Parks, S. and Wieschaus, E. (1998). Hyperactivation of the *folded gastrulation* pathway induces specific cell shape changes. *Development* **125**, 589-597.

Müller, H. A. J. and Wieschaus, E. (1996). *armadillo*, *bazooka*, and *stardust* are critical for early stages in formation of the zonula adherens and maintenance of the polarized blastoderm epithelium in *Drosophila*. *J. Cell Biol.* **134**, 149-163.

Oda, H. and Tsukita, S. (1999). Nonchordate classic cadherins have a structurally and functionally unique domain that is absent from chordate classic cadherins. *Dev. Biol.* **216**, 406-422.

Oda, H., Tsukita, S. and Takeichi, M. (1998). Dynamic behavior of the cadherin-based cell-cell adhesion system during *Drosophila* gastrulation. *Dev. Biol.* **203**, 435-450.

Oda, H., Uemura, T., Harada, Y., Iwai, Y. and Takeichi, M. (1994). A *Drosophila* homolog of cadherin associated with Armadillo and essential for embryonic cell-cell adhesion. *Dev. Biol.* **165**, 716-726.

Oda, H., Uemura, T., Shiomi, K., Nagafuchi, A., Tsukita, S. and Takeichi, M. (1993). Identification of a *Drosophila* homologue of α-catenin and its association with the *armadillo* protein. *J. Cell Biol.* **121**, 1133-1140.

Odell, G. M., Oster, G., Alberch, P. and Burnside, B. (1981). The mechanical basis of morphogenesis. I. Epithelial folding and invagination. *Dev. Biol.* **85**, 446-462.

Parks, S. and Wieschaus, E. (1991). The *Drosophila* gastrulation gene concertina encodes a Gα-like protein. *Cell* **64**, 447-458.

Pesacreta, T. C., Byers, T. J., Dubreuil, R., Kiehart, D. P. and Branton, D. (1989). *Drosophila* spectrin: the membrane skeleton during embryogenesis. *J. Cell Biol.* **108**, 1697-1709.

Provost, E. and Rimm, D. L. (1999). Controversies at the cytoplasmic face of the cadherin-based adhesion complex. *Curr. Opin. Cell Biol.* **11**, 567-572.

Robertson, H. M., Preston, C. R., Phillis, R. W., Johnson-Schlitz, D. M., Benz, W. K. and Engels, W. R. (1988). A stable genomic source of P-element transposase in *Drosophila melanogaster*. *Genetics* **118**, 461-470.

Schoenwolf, G. C. and Franks, M. V. (1984). Quantitative analysis of changes in cell shapes during bending of the avian neural plate. *Dev. Biol.* **105**, 257-272.

Steinberg, M. S. and McNutt, P. M. (1999). Cadherins and their connections: adhesion junctions have broader functions. *Curr. Opin. Cell Biol.* **11**, 554-560.

Sweeton, D., Parks, S., Costa, M. and Wieschaus, E. (1991). Gastrulation in *Drosophila*: The formation of the ventral furrow and posterior midgut invaginations. *Development* **112**, 775-789.

Tepass, U. (1999). Genetic analysis of cadherin function in animal morphogenesis. *Curr. Opin. Cell Biol.* **11**, 540-548.

Tepass, U., Gruszynski-DeFeo, E., Haag, T. A., Omatyar, L., Torok, T. and Hartenstein, V. (1996). *shotgun* encodes *Drosophila* E-cadherin and is preferentially required during cell rearrangement in the neuroectoderm and other morphogenetically active epithelia. *Genes Dev.* **10**, 672-685.

Tepass, U. and Hartenstein, V. (1994). The development of cellular junctions in the *Drosophila* embryo. *Dev. Biol.* **161**, 563-596.

Turner, F. R. and Mahowald, A. P. (1977). Scanning electron microscopy of *Drosophila melanogaster* embryogenesis. II. Gastrulation and segmentation. *Dev. Biol.* **57**, 403-416.

Uemura, T., Oda, H., Kraut, R., Hayashi, S., Kataoka, Y. and Takeichi, M. (1996). Zygotic *Drosophila* E-cadherin expression is required for processes of dynamic epithelial cell rearrangement in the *Drosophila* embryo. *Genes Dev.* **10**, 659-671.

Yap, A. S., Brieher, W. M. and Gumbiner, B. M. (1997). Molecular and functional analysis of cadherin-based adherens junctions. *Annu. Rev. Cell Dev. Biol.* **13**, 119-146.

Young, P. E., Pesacreta, T. C. and Kiehart, D. P. (1991). Dynamic changes in the distribution of cytoplasmic myosin during *Drosophila* embryogenesis. *Development* **111**, 1-14.